Desalination and Water Treatment
www.deswater.com
doi: 10.1080/19443994.2015.1017007

57 (2016) 7155–7165
April

Taylor & Francis
Taylor & Francis Group

Modeling the impacts of corrosion product formation on simultaneous sorption and reductive dehalogenation of organochlorine pesticide aldrin by high carbon iron filings (HCIF)

Yangdup Lama[a], Alok Sinha[a,*], Gurdeep Singh[a], Sanjeev Anand Sahu[b], Brijesh Kumar Mishra[a]

[a]*Department of Environmental Science and Engineering, Indian School of Mines, Dhanbad, Jharkhand 826004, India, Tel. +91 9572502513; email: yangla149@gmail.com (Y. Lama), Tel. +91 326 2235610; Fax: +91 326 2296624, 2296563; email: aloksinha11@yahoo.com (A. Sinha), Tel. +91 326 2235228; email: s_gurdeep2001@yahoo.com (G. Singh), Tel. +91 326 2235752; email: bkmishra3@rediffmail.com (B.K. Mishra)*
[b]*Department of Applied Mathematics, Indian School of Mines, Dhanbad, Jharkhand 826004, India, Tel. +91 326 2235917; email: ism.sanjeev@gmail.com*

Received 19 May 2014; Accepted 3 February 2015

ABSTRACT

The extensive use of organochlorine pesticides and their persistence in the environment has led to it becoming a major contaminant in the ground water and soil. This study concerns the interaction of organochlorine pesticide, aldrin, with high carbon iron filings (HCIF) and the impact of rusting on the performance of HCIF. Two types of HCIF were invesitagted: fresh (with no oxide coating) and rusted (with Fe(II)/Fe(III) oxide coatings). Substantial partitioning of aqueous-phase aldrin to the fresh HCIF surface was observed and the residual aqueous aldrin underwent slow reductive dehalogenation due to interaction with metallic iron. The overall rate of change of total aldrin concentration with time, i.e. (dC_t/dt), can be expressed as a function of aqueous concentration (C_a) as $-k_1 M (C_a)^n$, where M is the concentration of HCIF. The values of k_1 and n were determined to be 3.45×10^{-3} h^{-1} g^{-1} iron L and 3.115 for fresh, and 7.73×10^{-3} h^{-1} g^{-1} iron L and 2.572 for rusted HCIF, respectively. Equilibrium partitioning of aldrin between aqueous and solid phases in both the cases was described by Freundlich isotherm, $C_s = K [C_a]^m$, where m (1.485 fresh; 0.6985 rusted) and K (1.5×10^{-2} for fresh and 9.01×10^{-4} for rusted) were determined. Assuming desorption rate constants as 1 for fresh and 0.1 for rusted, the expressions developed for describing the evolution of C_s and C_a with time resulted in an adequate model fit to the experimental data. The rusting of HCIF decreased adsorption and reductive dehalogenation reactions, and was supported by X-ray diffraction, scanning electron microscopy, and energy dispersive X-ray spectroscopy data. The changes in the rate of reductive dehalogenation and adsorption of aldrin due to formation of iron oxides on the HCIF surface were observed in the present study.

Keywords: High carbon iron fillings; Aldrin; Iron oxide coating; Reductive dehalogenation; Sorption

*Corresponding author.

1. Introduction

The most commonly used organochlorine pesticides (OCP) in the developing countries of Asia are dichlorodiphenyltrichloroethane (DDT), hexachlorocyclohexane (HCH), aldrin, and deildrin [1,2] because of their effectiveness towards several pests and it is cost efficient. Due to their ability to bioaccumulate and resist degradation, OCP poses a serious threat to humans and wildlife as a potential toxin [3–6].

The use of zero-valent iron (ZVI) as an *in situ* remediation tool for the treatment of contaminated groundwater by the virtue of reductive dehalogenation of halogenated organic compounds has been a subject of considerable interest. Reports on the use of permeable reactive barrier (PRB) for *in situ* remediation of groundwater as the primary application of ZVI have been motivating [7,8]. HCIF is used as a reactive material in PRBs [9]. Several reports support the wide application of ZVI for dehalogenation of halogenated organic compounds [10–15]. Anaerobic conditions render the OCP non-persistent in contrast to the aerobic conditions which make them persistent [16,17]. Hence, the degradation of OCPs can be facilitated under reducing conditions [14]. ZVI can generate a reduced environment in water, soils, and sediments [18–21] and hence can operate as a powerful, inexpensive, and environmental friendly reducing agent for degradation of chlorinated contaminants. Numerous studies have been conducted that support the use of ZVI for DDT, and HCH degradation in soil and water [15,18,20,22,23].

The impacts of rusting on the dehalogenation process and the longevity of ZVI have been explored in some studies [24–28]. The formation of surface corrosion product such as ferrihydrite ($Fe_3HO_8{\cdot}4H_2O$), hematite (α-Fe_2O_3), and goethite (α-FeOOH) in aerobic conditions [29] and amorphous ferrous hydroxide ($Fe(OH)_2$) which transforms to magnetite (Fe_3O_4) under anoxic condition was reported to be formed on the ZVI surface [30,31]. These surface corrosion products may interfere with the dehalogenation of halogenated organic compounds by ZVI. The formations of iron corrosion products such as iron carbonate hydroxide, green rust, magnetite, ferrihydrite, maghemite, and hydrated ferric oxides such as akangite (*β*-FeOOH), goethite (α-FeOOH), and lepidocrocite (γ-FeOOH) have also been reported [26,32]. The formation of minerals such as siderite ($FeCO_3$), aragonite, calcite ($CaCO_3$), mackinawite, greigite, brucite ($Mg(OH)_2$), iron sulfide (FeS), and elemental sulfur have been reported, depending upon the different chemical environments surrounding the ZVI surface [25,26,32,33]. Such alterations of the ZVI surface can reduce permeability through ZVI media [34] and decrease the rates of dehalogenation of chlorinated organic compounds [35,36]. However, all iron oxides are not detrimental to the dehalogenation process as iron oxides such as green rust [24,37–39], magnetite [40,41], mackinawite [42,43], triolite [40], and pyrite [41] can facilitate the electron transfer. The presence of surface corrosion products such as maghemite, ferrihydrite, and goethite inhibits the dehalogenation reactions as they are poor electron donors [44].

Although the use of ZVI for degrading chlorinated organic compounds is well documented, the literature for application of ZVI for the degradation of OCPs like aldrin is very limited [45]. This study investigates the interaction of HCIF with aldrin, a persistent OCP, and the impact of its rusting on the rate and extent of dehalogenation of aldrin. The carbon present as graphite inclusions on HCIF may aid in the sorption of relatively hydrophobic aldrin, which has been identified as a priority pollutant by US Environmental Protection Agency [46]. In this study, the interaction of aldrin with two types of HCIF was examined: (1) with no initial surface oxide coating (fresh HCIF), and (2) with an initial surface oxide coating of mixed Fe(II)/Fe(III) oxides (rusted HCIF). The main objectives of the study were to (1) to determine the rate of aldrin degradation by fresh and rusted HCIF, (2) model the interaction of aldrin with the HCIFs, and (3) study the effect of rusting on the degradation of aldrin and elucidate the processes and mechanisms behind the observed results through X-ray diffraction (XRD), scanning electron microscopy (SEM), and energy dispersive X-ray spectroscopy (EDS).

2. Materials and methods

2.1. Chemicals

Chemicals used were aldrin (99%, Dr. Ehrenstorfer GmbH), methanol (99%, Emplura), n-hexane (Merck HPLC Grade, Mumbai, India), HCl (AR Grade, Ranken Reagent), and HNO_3 (AR Grade, Qualigens Fisher Scientific).

2.2. Preparation of HCIF

As per the procedure described by Sinha and Bose [47] commercially available high carbon iron (purchased at Dhanbad, Jharkhand, India) was chipped on a lathe machine and then grounded into iron filings in a ball mill. The fraction of filings passing through 425 μm (40 mesh) sieve and retained on 212 μm (80 mesh) sieve was used.

Two types of HCIF were prepared for the study. To prepare fresh HCIF samples with no surface rust, iron filings obtained as above was washed in nitrogen-sparged 1 N HCl with periodic shaking for 30 min, then rinsed 10–12 times with N_2-sparged deionized (Milli Q) water, and dried for 2 h at 100˚C under nitrogen atmosphere. This treatment yielded black metallic filings with no visible rust on the surface. To prepare rusted HCIF moist HCIF was kept in the oven (open atmosphere) at 500˚C for 10 h and cooled in an open atmosphere. Both types of HCIF were kept in a vacuum desiccator to prevent further changes in the surface characteristics.

2.3. HCIF characterization

The carbon content of fresh HCIF was determined by LECO, USA to be 3.05%. Surface area of fresh HCIF was determined by BET (N_2) analysis using a BET surface area analyzer (NOVA 4000e, Quantachrome, USA) to be 1.4 $m^2\ g^{-1}$.

XRD analyses were carried out for the surface characterization of both of the HCIF surfaces. X-ray powder diffractometer (Bruker D_8 Focus), using Cu-K_α radiation (with $\lambda = 1.541$ Å), was employed for this purpose. The scan rate used was $3^\circ\ min^{-1}$. The diffraction patterns were analyzed using DIFFRAC^{plus} (Release 2001 Eva version 7.0) software.

Scanning electron micrographs of fresh HCIF and rusted HCIF were obtained using a SEM (FE-SEM-Zeiss, Supra 65) operating at an accelerating voltage of 5 kV, working distance 3.5 mm, and the magnification of the samples were fixed at 5–6 K×. The SEM was equipped with EDS facility and the element characterizations were done at four points for each sample.

2.4. Experimental procedure

The experiments were carried out in batch reactors of 20 mL glass vials with screw caps equipped with teflon lined resealable rubber septa (Agilent India). To each vial, approximately 5 g of fresh HCIF or rusted HCIF was added. No efforts were made to control the pH. Aqueous solution of aldrin (1 mg L^{-1}) was prepared by adding the required volume of pesticide in methanol to deionized (Milli Q) water sparged with N_2 and transferred to 1 L separation funnel and was sparged with N_2 to maintain the anoxic conditions. The vials containing HCIF were filled by the funnel in such a way to prevent any headspace. Control vials containing aldrin solution, but no HCIF, were also prepared. The vials were placed on a rotator and rotated at 30 rpm such that the vial axis remained horizontal at all times. The batch experiments were carried out in an ambient temperature of 25 ± 1˚C. The vials were removed (in duplicate and one control) at specified times, ranging from 1 to 384 h.

2.5. Analytical procedure

The pH and oxidation–reduction potential (ORP) of the aqueous phase in all vials were recorded after the sampling of the vials. Waterproof pH Tester 30 (Eutech Instruments, Okalon), ORP Tester 10, and 10 BNC (Eutech Instruments, Okalon) were employed for this purpose.

Both the aqueous and sorbed aldrin concentrations were measured in all vials where aldrin was in contact with iron filings. At specified time intervals, 1 mL aliquots of aqueous phase were withdrawn from the batch reactors, using a microsyringe pierced through the septa. A 0.5 mL aliquot was added to a gas chromatography (GC) auto sampler vial (Wheaton Science, USA) containing 1.5 mL n-hexane and sealed. The mixture was then thoroughly mixed on a vortex mixer for 30 min to ensure partitioning of aldrin into the solvent phase. This method resulted in 97% extraction efficiency of aldrin. The solvent extract was analyzed by GC. For determining solid-phase aldrin concentration, aqueous content of the 20 mL vial was transferred to another vial, by using a cannula, and the decanted vials are weighed for determination of the amount of sorbed pesticide solution. About 10 mL of n-hexane was added to this vial and the contents were vortex mixed for 5 min to ensure transfer of the solid-phase aldrin to the solvent. The concentration of aldrin in this solvent was determined by GC.

A Thermo Scientific Ceres 800 GC with a split/splitless mode equipped with capillary column DB-5MS (30 m × 0.25 mm × 0.25 μm) was used for analysis of aldrin. Carrier gas used was N_2 maintained at a flow rate of 1.2 ml/min. The temperature of ECD detector was maintained at 300˚C and the injector port at 275˚C. The oven temperature program was as follows: starting at 160˚C (0 min), ramp at $7^\circ C\ min^{-1}$ to 320˚C (0 min). Samples 1 μL were injected at splitless mode. The detection limit of aldrin was 1.8 pg μL^{-1}, and the corresponding signal/noise ratio (S/N) was greater than 5.

3. Model development

The model used to validate the findings of this paper has been adapted from the model that was used to understand the interaction between 2-chloronaphthalene and HCIF [46]. The partitioning of aqueous-phase aldrin molecules to carbon present on the HCIF surface is likely to occur during the interaction of the

aldrin with HCIF. This is immediately followed by the reductive dehalogenation of the residual aqueous aldrin through the interaction with metallic iron. The overall decrease in the aldrin concentration due to dehalogenation is responsible for the readjustment of aldrin partitioning between solid and aqueous phases.

At any time during the interaction of aldrin with HCIF in batch systems,

$$C_t\ (\mu\text{moles L}^{-1}) = [C_s\ (\mu\text{moles g}^{-1}\ \text{iron})\ M\ (\text{g iron L}^{-1})] + C_a\ (\mu\text{moles L}^{-1}) \quad (1)$$

where C_a (μmoles L^{-1}), C_s (μmoles g^{-1} iron), and C_t (μmoles L^{-1}) are the aqueous, sorbed, and total aldrin concentrations and M (g iron L^{-1}) is the concentration of HCIF. The decrease in total aldrin concentration, C_t with time, due to dehalogenation through interaction with the metallic iron surface is represented as,

$$n \cdot C_a + M \rightarrow \text{Deha log enation products} \quad (2)$$

therefore, rate of change of total aldrin concentration,

$$\frac{dC_t}{dt} = -k_1 M\ (C_a)^n \quad (2a)$$

Eq. (2a) can be expressed in the linearized form as,

$$\ln\left[-\frac{dC_t}{dt}\right] = \ln[Mk_1] + n\ln[C_a] \quad (2b)$$

The rate of dehalogenation of aldrin, k_1 (L h^{-1} g^{-1} iron), and the order of the reaction n, can be determined from a plot of $\ln\left[-\frac{dC_t}{dt}\right]$ vs. $\ln[C_a]$. The partitioning of aldrin on HCIF is assumed to be non-specific in nature i.e. the number of site available for adsorption is restricted only by the number of aldrin molecules that can be adsorbed on the carbon present on the HCIF surface [28]. At low-surface coverage, such partitioning can be represented as

$$mC_a(\mu\text{moles L}^{-1}) + M(\text{g iron L}^{-1}) \underset{k_3}{\overset{k_2}{\rightleftarrows}} c_s\ (\mu\text{mole L}^{-1}), \quad (3)$$

where $c_s = MC_s$

Where k_2, and k_3 are adsorption and desorption rate constants, respectively. Assuming the rate of partitioning is fast in comparison to dehalogenation reactions; adsorption equilibrium was assumed to be maintained at all times after the start of aldrin interaction with HCIF. The corresponding equilibrium constant describing aldrin partitioning is $K = k_2/k_3$. Under such conditions, partitioning of aldrin between solid and aqueous phases can be represented by a Freundlich isotherm,

$$C_s = K\ [C_a]^m \quad (4)$$

A linearized form of Eq. (4) can be expressed as,

$$\ln\ C_s = m\ \ln[C_a] + \ln K \quad (4a)$$

Eq. (4(a)) is utilized to determine the equilibrium constant K and the Freundlich exponent, m. Now the rate of change in aqueous aldrin concentration, $\frac{dC_a}{dt}$, can be represented as, $\frac{dC_a}{dt}$ = (Rate of desorption of aldrin from the solid phase to aqueous phase) − (Rate of adsorption of aldrin from the aqueous to the solid phase) − (Rate of dehalogenation of aldrin in aqueous phase) or,

$$\frac{dC_a}{dt} = k_3 M[C_s] - k_2 M[C_a]^m - k_1 M[C_a]^n \quad (5)$$

From Eqs. (1), (2(a)) and (5), the rate of change of sorbed aldrin can be represented as,

$$\frac{dCs}{dt} = k_3[C_s] - k_2[C_a]^m \quad (6)$$

4. Results and discussion

4.1. X-ray diffraction

The prominent peaks consistent with metallic iron were observed in the XRD spectra of fresh HCIF surface (Fig. 1a) as inferred from JC-PDF: 06-696 (2θ values 44.671, 65.018, 82.329, and 98.940). No additional peaks, attributing to the presence of iron oxides, were observed. However, in the XRD spectra of the rusted HCIF surface (Fig. 1b), peaks consistent with magnetite (JC-PDF: 19-0629) (2θ values 30.095, 35.442, 62.515, 56.942, and 73.948), maghemite (JC PDF: 25-1402) (2θ values 35.327, 41.715, 67.841, and 74.783), and hematite (JC-PDF: 33-0664) (2θ values 24.138, 33.157, 35.612, 49.480, 54.091, and 62.421) were observed. No peak attributing to the presence of metallic iron was observed. The surface coating of rusted HCIF by iron oxides can be established by the results of XRD.

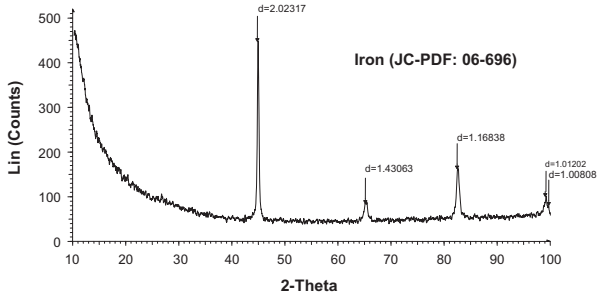

Fig. 1a. X-ray diffraction results for fresh HCIF.

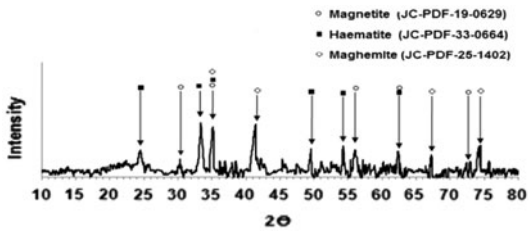

Fig. 1b. X-ray diffraction results for rusted HCIF.

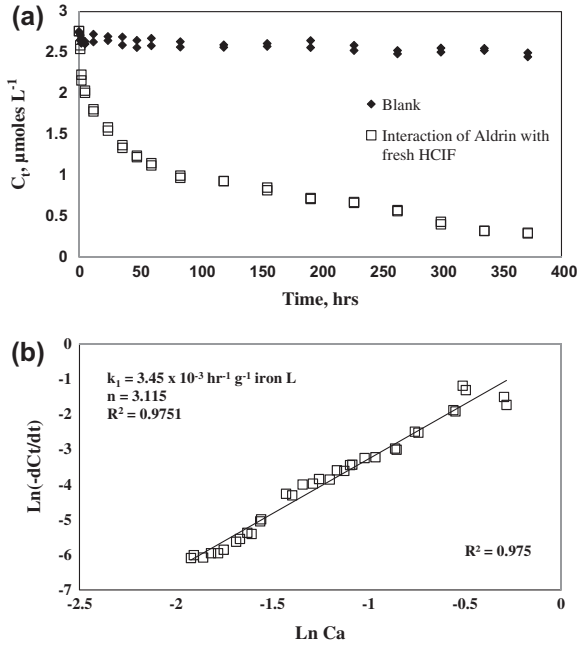

Fig. 2. Interaction of aldrin with fresh HICF (a) Decline in total concentration of aldrin with time and (b) linearized plot of aldrin degradation vs. aqueous-phase concentration of aldrin.

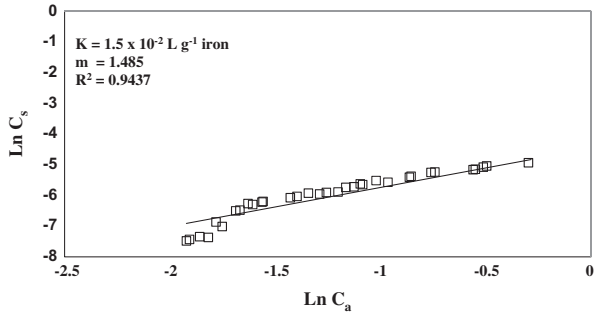

Fig. 3. Linearized plot for Freundlich isotherm describing the equilibrium partitioning of aldrin between solid and aqueous phase during interaction with fresh HCIF.

4.2. Interaction of aldrin with fresh HCIF

Aldrin was contacted with the two types of HCIF (fresh and rusted), in batch reactors, for the specified time interval as described in Section 2.4. During the course of experiment with fresh HCIF, the pH and ORP was observed to vary between 7.5 and 10.5 and −450 to −600 mV, respectively.

During the interaction of aldrin with fresh HCIF, the total concentration of aldrin (C_t, µmoles L^{-1}) declined as presented in Fig. 2(a). The kinetic coefficients k_1 and n, as evaluated from a plot of ln ($-dC_t/dt$) vs. ln C_a (Fig. 2(b)), were 3.45×10^{-3} L hr^{-1} g^{-1} iron and 3.1115, respectively. A linear fit was also observed for the plot of ln C_s vs. ln C_a (Fig. 3), suggesting equilibrium was established between the aqueous- and sorbed-phase aldrin, which could be explained by Freundlich isotherm. The constants obtained from Freundlich isotherm were $m = 1.485$ and $K = 1.5 \times 10^{-2}$.

The partitioning of aldrin on HCIF surface and the simultaneous reductive dehalogenation of aqueous aldrin can be explained by the model given above. Eqs. (1), (2(a)) and (6) depicting the model were solved simultaneously using ODE23, ordinary differential equation solver MATLAB R2009b. The following initial conditions were used, at time $t = 0$, $C_a = C_t = 2.76$ µmoles L^{-1}. M was taken as 250 g L^{-1}. The values of k_1, n, and m determined from the respective plots were used to obtain the variation of C_a, C_t, and C_s with time. The known value of K is expressed as a ratio of k_2/k_3, the unknown values of adsorption rate and desorption rate, respectively. Various values of k_3 were assumed until the numerical solution for temporal variation of C_a, C_t, and C_s matched with the experimental data.

The experimental and corresponding model simulations for total aldrin concentration (C_t), aqueous aldrin concentration (C_a), and sorbed aldrin concentration (C_s) are depicted in Fig. 4(a)–(c), respectively. The inset diagram in Fig. 4(b) is for the initial data points up to $t = 72$ h to represent the agreement between model and experimental data. A general overall

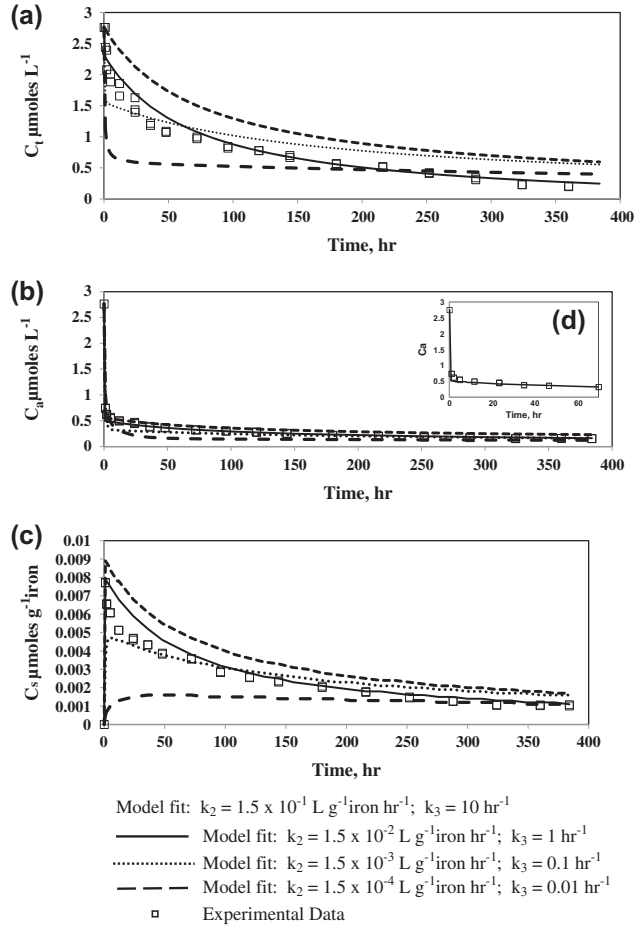

Fig. 4. Mathematical simulation of interaction of aldrin with pure HCIF (a) total concentration of aldrin, (b) aqueous concentration of aldrin, (c) sorbed concentration of aldrin, and (d) magnified view of aqueous concentration showing model fit.

decline was observed for total aldrin concentration, initial rapid decline followed by slower decline in the aqueous phase, and initial increase followed by slow decline was observed for the sorbed aldrin concentration. The mathematical simulation corresponding to $k_3 = 1$ and $k_2 = 1.5 \times 10^{-2}$ was observed to fit the experimental data adequately. The other values of k_3 and k_2 correspond to a condition where the partitioning reactions and the reductive dehalogenation reactions are not coherent with our findings. Hence, the rate of change of aqueous aldrin concentration, for interaction of aldrin with fresh HCIF, can be expressed as,

$$\frac{dC_a}{dt} = 1 \cdot M \cdot [C_s] - 0.0152 \cdot M \cdot [C_a]^{1.485} - 0.00345 \cdot M \cdot [C_a]^{3.115} \quad (7)$$

4.3. Interaction of aldrin with rusted HCIF

The variation in pH and the ORP recorded during the experimental period were 6.5–7.5 and −150 to −200 mV, respectively. The increase in pH during the interaction of aldrin with rusted HCIF was not as high as observed during the interaction with fresh HCIF. This may be attributed to the fact that due to higher corrosion of HCIF surface and development of oxide layer, further oxidation of HCIF is reduced, which leads to decline in reduction of water and hence OH^- production. Similarly, the ORP values have increased compared to the fresh HCIF case, which indicates the decline in reduction capacity of HCIF. The decline in the total concentration of aldrin (C_t) with time, during its interaction with rusted HCIF, is presented in Fig. 5(a). As in the earlier case, a straight line for the plot of ln ($-dC_t/dt$) vs. ln C_a (Fig. 5(b)) was obtained, and the rate constant (k_1) and the reaction order (n) were obtained to be 7.73×10^{-5} L h^{-1} g^{-1} iron and 2.572, respectively. The Freundlich isotherm could also be applied to explain the equilibrium established between the aqueous concentration and the sorbed concentration as shown in Fig. 6, and the corresponding Freundlich constants were $K = 9.01 \times 10^{-4}$ and $m = 0.6985$, respectively.

The numerical solutions of the Eqs. (1), (2(a)) and (6) for various assumed values of k_3 along with the

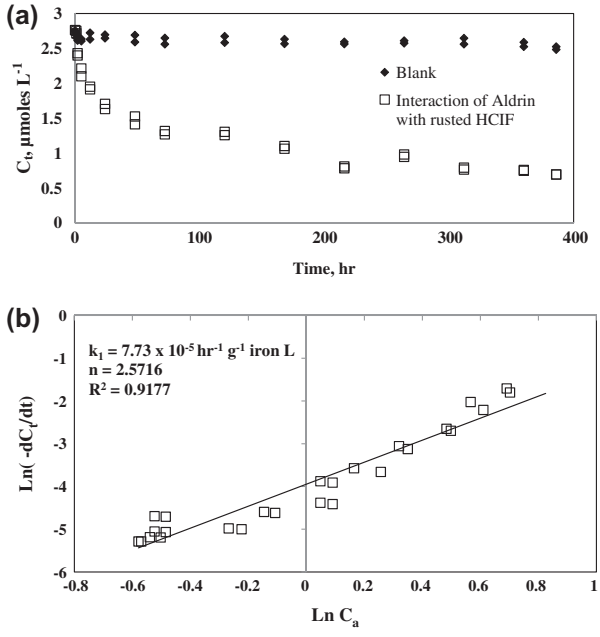

Fig. 5. Interaction of aldrin with rusted HICF (a) decline in total concentration of aldrin with time and (b) linearized plot of aldrin degradation vs. aqueous-phase concentration of aldrin.

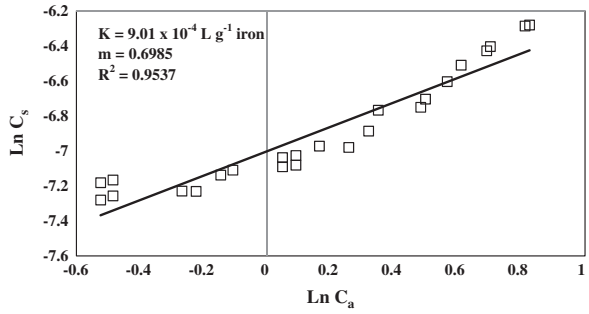

Fig. 6. Linearized plot for Freundlich isotherm describing the equilibrium partitioning of aldrin between solid and aqueous phase during interaction with rusted HCIF.

experimental data for C_t, C_a, and C_s are given in Fig. 7(a)–(c), respectively. Similar to the interaction with fresh HCIF a general overall decline was observed for C_t, initial rapid decline followed by slower decline for C_a and initial increase followed by slow decline was observed for C_s. The simulation corresponding to $k_2 = 9.01 \times 10^{-5}$ and $k_3 = 0.1$ was

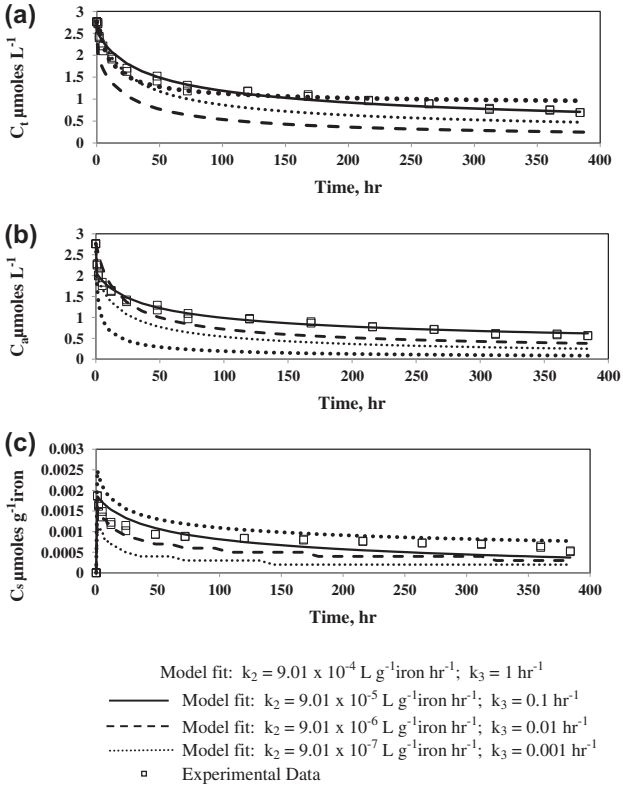

Fig. 7. Mathematical simulation of interaction of aldrin with rusted HCIF (a) total concentration of aldrin (b) aqueous concentration of aldrin and (c) sorbed concentration of aldrin.

observed to fit the experimental data adequately. Hence, the rate of change of aqueous aldrin concentration, during the interaction of aldrin with rusted HCIF, can be expressed as,

$$\frac{dC_a}{dt} = 0.1 \cdot M \cdot [C_s] - 0.0000901 \cdot M \cdot [C_a]^{0.6985} - 0.0000773 \cdot M \cdot [C_a]^{2.572} \quad (8)$$

4.4. Discussion

The degradation of DDT and HCH by ZVI have been reported to follow pseudo-first-order kinetics [15,18], which is not consistent with our results. Pure zero-valent iron was used in their studies which was devoid of any graphite inclusion; hence, it did not incorporate the sorption phenomena in the reductive dehalogenation process. In the present study, the presence of sorption equilibrium, which further governed the reductive dehalogenation taking place in the aqueous phase, led to the development of a complex set of reactions, hence cannot be compared. The higher apparent order of the reaction (3.115 for fresh HCIF and 2.572 for rusted HCIF) can be attributed to the complex coupling of adsorption–desorption with dehalogenation.

The mathematical simulation of the interaction of aldrin with both fresh and rusted HCIF indicates that the partitioning reactions are faster than reductive dehalogenation reactions. This can be supported by the results tabulated in Table 1, where the k_2 and k_3 values are higher than the k_1 values in both the cases. Adsorption of aldrin to the HCIF surface (fresh and rusted) can be described by Freundlich isotherms and is governed by the carbon content present on both the HCIF surfaces. The reductive dehalogenation reaction by ZVI is a surface-mediated phenomenon [47] and is affected by the solubility of the contaminants [15]. The high octanol/water partition coefficient of 5.3 [48] renders higher adsorption of aldrin to HCIF which leads to low aqueous concentration of aldrin and subsequently low reductive dehalogenation rates in fresh HCIF in comparison to adsorption–desorption rates.

As per the comparison of data given in Table 1, both the partition rates and the reductive dehalogenation rates were observed to be smaller in the case of rusted HCIF than fresh HCIF. This can be attributed to the presence of iron oxides on the rusted HCIF surface. The presence of iron oxides leads to a reduction in the carbon content and metallic iron content on the HCIF surfaces. Visible cracks and crevices are observed in the SEM image of fresh HCIF (Fig. 8a).

Table 1
Comparison of partitioning and dehalogenation reactions of aldrin interaction with fresh HCIF and rusted HCIF

	Partitioning reaction				Dehalogenation reaction	
Parameters	Freundlich equilibrium constant (K)	Freundlich exponent (m)	Adsorption rate constant (k_2)	Desorption rate constant (k_3)	Order of reaction (n)	Dehalogentaion rate (k_1) (L g^{-1} iron h^{-1})
Fresh HCIF	1.5×10^{-2}	1.485	1.5×10^{-2}	1	3.115	3.45×10^{-3}
Rusted HCIF	9.01×10^{-4}	0.6985	9.01×10^{-5}	0.1	2.572	7.73×10^{-5}

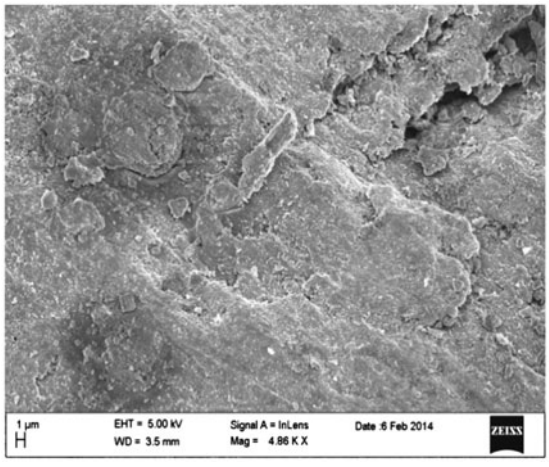

Fig. 8a. Scanning electron micrographs for fresh HCIF (magnification: 4.86 K×).

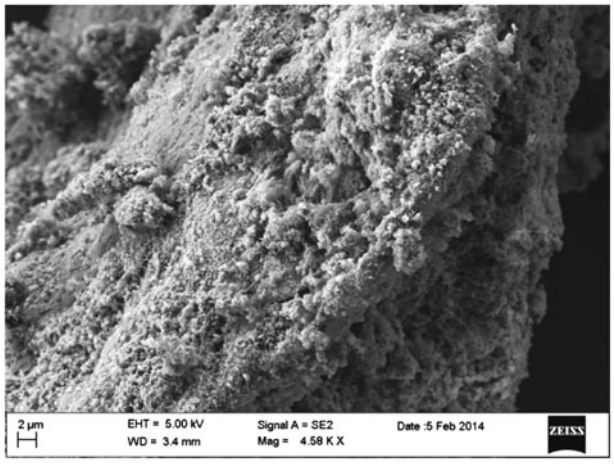

Fig. 8b. Scanning electron micrographs for rusted HCIF (magnification: 4.59 K×).

However, the SEM image of rusted HCIF (Fig. 8b) indicates considerable changes in the surface morphology where the entire surface is appeared to be covered by a rough canopy. The EDS results obtained for fresh HCIF and rusted HCIF surfaces are presented in Table 2. Abundance of iron, specific amount of carbon, and the meager amount of oxygen were observed on the fresh HCIF surface as compared to considerable increase in oxygen and decrease in iron and carbon for rusted HCIF. These results are consistent with the presence of iron oxides magnetite, maghemite, and hematite on the surface of rusted HCIF as indicated by the XRD results. Sinha and Bose [28] similarly observed slower chloronapthalene adsorption and dehalogenation on rusted HCIF. As evident from Table 2, the carbon surface in rusted HCIF declined by 55% in comparison to fresh HCIF. Similarly, the amount of aldrin adsorbed to rusted HCIF also declined by about 72% in comparison to fresh HCIF. Hence, it may be concluded that the adsorption of aldrin took place to these graphite inclusion (carbon surface) present on fresh HCIF and rusted HCIF.

The presence of iron oxides on the HCIF surfaces can also adversely affect the reductive dehalogenation reaction by altering the electron transfer mechanism. Though, the presence of magnetite, exhibiting semiconductor characteristics [49–51], does not have substantial impact, it is the presence of hematite exhibiting insulating character [44] which inhibits the electron transfer, thereby contributing to retarding the reductive dehalogenation process. As it is clear from SEM micrographs of rusted HCIF (Fig. 8b) that the reactive and non-reactive sites are all covered by oxide surfaces, still the reductive dehalogenation process continues. This may be attributed to the presence of magnetite, as evident from XRD, which allows transfer of electrons.

It can be noted that the HCIF surface is dry before the addition of pesticide solution. The HCIF surface is very slowly transformed once in contact with the aqueous aldrin solution. Thus, the surfaces of both fresh and rusted HCIF are unlikely to change significantly during the course of the experiment.

Table 2
Energy-dispersive X-ray spectrometry results for fresh HCIF and rusted HCIF

Fresh HCIF			Rusted HCIF		
Element	Weight percent	Atomic percent	Element	Weight percent	Atomic percent
Carbon	6.5	23.5	Carbon	2.9	6.4
Oxygen	2.1	5.6	Oxygen	40.2	66.6
Iron	91.4	70.8	Iron	56.9	27.0

5. Summary and conclusions

The current study investigated the performance of rusted HCIF and thus evaluated the long-term performance of a HCIF PRB constructed for treatment of OCP like aldrin. Specifically, the main conclusions of this study were the following,

- The initial rapid partitioning of aldrin on the solid phase was observed due to adsorption on the graphite inclusions present on HCIF, while the residual aqueous phase was observed to undergo simultaneous reductive dehalogenation through the interaction with metallic iron. The process was validated by developing a mathematical model to describe the interaction of aldrin with fresh as well as rusted HCIF.
- The Freundlich isotherm's parameter reported for the interaction of aldrin with fresh HCIF were $K = 1.5 \times 10^{-2}$ and $m = 1.485$. The reductive dehalogenation rate constant $k_1 = 3.45 \times 10^{-3}$ L h^{-1} g^{-1} iron and reaction order $n = 3.115$ were reported. Considering K to be the ratio of the rates of adsorption (k_2) and desorption (k_3), the above isotherm and dehalogenation parameters determined were utilized for the simulation of the composite interaction of the two HCIF surfaces with aldrin. Mathematical simulation corresponding to $k_2 = 1.5 \times 10^{-2}$ and $k_3 = 1$ for fresh HCIF were observed to adequately fit the experimental data.
- The extent of aldrin adsorption on the rusted HCIF surface and its corresponding dehalogenation rate in the aqueous phase was observed to be reduced. The adsorption can be described by Freundlich isotherm with parameters $K = 9.01 \times 10^{-4}$ and $m = 0.6985$, respectively. The dehalogenation rate constant $k_1 = 7.73 \times 10^{-5}$ L h^{-1} g^{-1} iron and order $n = 2.572$ were reported in the present study. Mathematical simulation corresponding $k_2 = 9.01 \times 10^{-5}$ and $k_3 = 0.1$ for rusted HCIF was observed to adequately fit the experimental data. The presence of iron oxides like magnetite, hematite, and meghamite as inferred by the XRD, SEM, and EDS investigations shielded both the reactive metallic site and the carbon content of the HCIF resulting in the decline in reductive dehalogenation and adsorption of aldrin on the HCIF surface.

Hence, it may be concluded that during the course of time, the formation of corrosion products on the HCIF surface, will affect the long-term performance of PRB. With anaerobic condition prevailing in the groundwater, the development of the oxide layer on HCIF surface may be slow; in case of corrosion product formation on HCIF surface, both the rate of adsorption and the rate of reductive dehalogenation of chlorinated contaminants will be reduced.

Acknowledgments

The authors heartily acknowledge ISM authorities for providing all necessary assistance, under the research project FRS (1)/2009-2010/1/ESE, for completion of this research work.

References

[1] P. Lallas, The stockholm convention on persistent organic pollutants, Am. J. Int. Law 95 (2001) 692–708.
[2] P.K. Gupta, Pesticide exposure-Indian scene, Toxicology 198 (2004) 83–90.
[3] K.C. Jones, P. de Voogt, Persistent organic pollutants (POPs): State of the science, Environ. Pollut. 100(1–3) (1999) 209–221.
[4] V. Turusov, V. Rakitsky, L. Tomatis, Dichlorodiphenyltrichloroethane (DDT): Ubiquity, persistence, and risks, Environ. Health Perspect. 110 (2002) 125–128.
[5] R.D. Behrooz, A.E. Sari, N. Bahramifar, S.M. Ghasempouri, Organochlorine pesticide and polychlorinated biphenyl residues in human milk from the Southern Coast of Caspian Sea Iran, Chemosphere 74 (2009) 931–937.
[6] A. Trejo-Acevedo, F. Díaz-Barriga, L. Carrizales, G. Domínguez, R. Costilla, I. Ize- Lema, M. Yarto-Ramírez, A. Gavilán-García, J.J. Jesús Mejía-Saavedra, I.N. Pérez- Maldonado, Exposure assessment of persistent

organic pollutants and metals in Mexican children, Chemosphere, 74 (2009) 974–980.
[7] R.W. Gillham, S.F. O'Hannesin, Enhanced degradation of halogenated aliphatics by zero-valent iron, Ground Water 32 (1994) 958–967.
[8] R.W. Puls, D.W. Blowes, R.W. Gillham, Long-term performance monitoring for a permeable reactive barrier at the U.S. Coast Guard Support Center, Elizabeth City, North Carolina, J. Haz. Mater. 68 (1999) 109–124.
[9] D.R. Burris, T.J. Campbell, V.S. Manoranjan, Sorption of trichloroethylene and tetrachloroethylene in a batch reactive metallic iron-water system, Environ. Sci. Technol. 29 (1995) 2850–2855.
[10] N. Kluyev, A. Cheleptchikov, E. Brodsky, V. Soyfer, V. Zhilnikov, Reductive dechlorination of polychlorinated dibenzo-p-dioxins by zerovalent iron in subcritical water, Chemosphere 46 (2002) 1293–1296.
[11] P.J. Shea, T.A. Machacek, S.D. Comfort, Accelerated remediation of pesticide-contaminated soil with zero-valent iron, Environ. Pollut. 132 (2004) 183–188.
[12] R. Cheng, J.L. Wang, W.X. Zhang, Comparison of reductive dechlorination of p-chlorophenol using Fe^0 and nanosized Fe^0, J. Hazard. Mater. 144 (2007) 334–339.
[13] J.H. Kim, P.G. Tratnyek, Y.S. Chang, Rapid dechlorination of polychlorinated dibenzo-p-dioxins by bimetallic and nanosized zerovalent iron, Environ. Sci. Technol. 42(11) (2008) 4106–4112.
[14] T. Satapanajaru, P. Anurakpongsatorn, A. Songsasen, H. Boparai, J. Park, Using low-cost iron byproducts from automotive manufacturing to remediate DDT, Water Air Soil Pollut. 175 (2006) 361–374.
[15] X. Cong, N. Xue, S. Wang, K. Li, F. Li, Reductive dechlorination of organochlorine pesticides in soils from an abandoned manufacturing facility by zero-valent iron, Sci. Total Environ. 408 (2010) 3418–3423.
[16] J.M. Aislabie, N.K. Richards, H.L. Boul, Microbial degradation of DDT and its residues–A review, New Zeal. J. Agr. Res. 40 (1997) 269–282.
[17] M.H.A. Van Eekert, N.J.P. Van Ras, G.H. Mentink, H.H.M. Rijnaarts, A.J.M. Stams, J.A. Field, G. Schraa, Anaerobic transformation of β-hexachlorocyclohexane by methanogenic granular sludge and soil microflora, Environ. Sci. Technol. 32 (1998) 3299–3304.
[18] G.D. Sayles, G.R. You, M.X. Wang, M.J. Kupferle, DDT, DDD, and DDE dechlorination by zero-valent iron, Environ. Sci. Technol. 31 (1997) 3448–3454.
[19] S.D. Comfort, P.J. Shea, T.A. Machacek, H. Gaber, B.T. Oh, Field-scale remediation of a metolachlor-contaminated spill site using zerovalent iron, J. Environ. Qual. 30 (2001) 1636–1643.
[20] T. Eggen, A. Majcherczyk, Effects of zero-valent iron (Fe^0) and temperature on the transformation of DDT and its metabolites in lake sediment, Chemosphere 62 (2006) 1116–1125.
[21] F.X. Yao, X. Jiang, G.F. Yu, F. Wang, Y.R. Bian, Evaluation of accelerated dechlorination of p,p´-DDT in acidic paddy soil, Chemosphere 64 (2006) 628–633.
[22] S.C. Yang, M. Lei, T.B. Chen, X.Y. Li, Q. Liang, C. Ma, Application of zerovalent iron (Fe^0) to enhance degradation of HCHs and DDX in soil from a former organochlorine pesticides manufacturing plant, Chemosphere 79 (2010) 727–732.
[23] Y.S. El-Temsah, E.J. Joner, Effects of nano-sized zero-valent iron (nZVI) on DDT degradation in soil and its toxicity to collembola and ostracods, Chemosphere 92 (2013) 131–137.
[24] M. Erbs, H.C.B. Bruun Hansen, C.E. Olsen, Reductive dechlorination of carbon tetrachloride using iron(II) iron(III) hydroxide sulfate (green rust), Environ. Sci. Technol. 33 (1999) 307–311.
[25] Y. Roh, S.Y. Lee, M.P. Elless, Characterization of corrosion products in the permeable reactive barriers, Environ. Geol. 40 (2000) 184–194.
[26] Y. Furukawa, J. Kim, J. Watkins, R.T. Wilkin, Formation of ferrihydrite and associated iron corrosion products in permeable reactive barriers of zero-valent iron, Environ. Sci. Technol. 36 (2002) 5469–5475.
[27] A. Sinha, P. Bose, Interaction of chloroethanes and chloroethenes with unrusted and rusted high carbon iron filings, Environ. Eng. Sci. 26 (2009) 61–70.
[28] A. Sinha, P. Bose, 2-chloronaphthalene dehalogenation by high-carbon iron filings: Formation of corrosion products on high-carbon iron filings surface, Environ. Eng. Sci. 28 (2011) 701–710.
[29] S.L.S. Stipp, M. Hansen, R. Kristensen, M.F. Hochella, L. Bennedsen, K. Dideriksen, T. Balic-Zunic, D. Léonard, H.J. Mathieu, Behaviour of Fe-oxides relevant to contaminant uptake in the environment, Chem. Geol. 190 (2002) 321–337.
[30] M.S. Odziemkowski, T.T. Schuhmacher, R.W. Gillham, E.J. Reardon, Mechanism of oxide film formation on iron in simulating groundwater solutions: Raman spectroscopic studies, Corros. Sci. 40 (1998) 371–389.
[31] P.M.L. Bonin, W. Jędral, M.S. Odziemkowski, R.W. Gillham, Electrochemical and Raman spectroscopic studies of the influence of chlorinated solvents on the corrosion behaviour of iron in borate buffer and in simulated groundwater, Corros. Sci. 42 (2000) 1921–1939.
[32] T. Kohn, K.J.T. Livi, A.L. Roberts, P.J. Vikesland, Longevity of granular iron in groundwater treatment processes: Corrosion product development, Environ. Sci. Technol. 39 (2005) 2867–2879.
[33] S. Yabusaki, K. Cantrell, B. Sass, C. Steefel, Multicomponent reactive transport in an in situ zero-valent iron cell, Environ. Sci. Technol. 35 (2001) 1493–1503.
[34] P.J. Vikesland, J. Klausen, H. Zimmermann, A.L. Lynn Roberts, W.P. Ball, Longevity of granular iron in groundwater treatment processes: Changes in solute transport properties over time, J. Contam. Hydrol. 64 (2003) 3–33.
[35] T.L. Johnson, M.M. Scherer, P.G. Tratnyek, Kinetics of halogenated organic compound degradation by iron metal, Environ. Sci. Technol. 30 (1996) 2634–2640.
[36] N. Ruiz, S. Seal, D. Reinhart, Surface chemical reactivity in selected zero-valent iron samples used in groundwater remediation, J. Hazard. Mater. B 80 (2000) 107–117.
[37] S. Loyaux-Lawniczak, P. Refait, J. Ehrhardt, P. Lecomte, J.R. Génin, Trapping of Cr by formation of ferrihydrite during the reduction of chromate ions by Fe(II)−Fe(III) hydroxysalt green rusts, Environ. Sci. Technol. 34 (2000) 438–443.
[38] A.G.B. Williams, M.M. Scherer, Kinetics of Cr(VI) reduction by carbonate green rust, Environ. Sci. Technol. 35 (2001) 3488–3494.

[39] W. Lee, B. Batchelor, Abiotic reductive dechlorination of chlorinated ethylenes by iron-bearing soil minerals. 2. green rust, Environ. Sci. Technol. 36 (2002) 5348–5354.
[40] T.M. Sivavec, D.P. Horney, Reduction of chlorinated solvents by Fe (II) minerals, in: Proceedings, 213th ACS Nat. Meet. Am. Chem. Soc., April 1997, San Francisco, CA, pp. 115–117.
[41] W. Lee, B. Batchelor, Abiotic reductive dechlorination of chlorinated ethylenes by iron-bearing soil minerals. 1. pyrite and magnetite, Environ. Sci. Technol. 36 (2002) 5147–5154.
[42] E.C. Butler, K.F. Hayes, Kinetics of the transformation of trichloroethylene and tetrachloroethylene by iron sulfide, Environ. Sci. Technol. 33 (1999) 2021–2027.
[43] E.C. Butler, K.F. Hayes, Kinetics of the transformation of halogenated aliphatic compounds by iron sulfide, Environ. Sci. Technol. 34 (2000) 422–429.
[44] J.E.O. Mayne, J.W. Menter, M.J. Pryor, 630. The mechanism of inhibition of the corrosion of iron by sodium hydroxide solution, J. Chem. Soc. (1950) 3229–3236.
[45] J. Hara, Y. Kawabe, T. Komai, C. Inoue, Chemical degradation of dieldrin using ferric sulfide and iron powder, Int. J. of Environ. Sci. Eng. 1–2 (2009) 91–96.
[46] US Environmental Protection Agency, Water quality standards database EPA numeric criteria, EPA criteria, effective date 27th Dec 2002, Available from: http://water.epa.gov/scitech/swguidance/standards/criteria/current/index.cfm.
[47] A. Sinha, P. Bose, Dehalogenation of 2-chloronaphthalene by cast iron, Water Air Soil Pollut. 172 (2006) 375–390.
[48] V. Zitko, The Handbook of Environmental Chemistry. Springer-Verlag, Berlin, 2003, pp. 47–90.
[49] P. Schmuki, M. Buchler, S. Virtanen, H. Bohni, Bulk metal oxides as a model for the electronic properties of passive films, J. Electrochem. Soc. 142 (1995) 3336–3342.
[50] B.A. Balko, P.G. Tratnyek, Photoeffects on the reduction of carbon tetrachloride by zero-valent iron, J. Phys. Chem. B 102 (1998) 1459–1465.
[51] J. Farrell, M. Kason, N. Melitas, T. Li, Investigation of the long-term performance of zero-valent iron for reductive dechlorination of trichloroethylene, Environ. Sci. Technol. 34 (2000) 514–521.